End debonding of CFRP wraps and strips for the strengthening of concrete structures

Pierluigi Colombi *, Giulia Fava, Carlo Poggi

Architecture, Built Environment and Construction Engineering, Politecnico di Milano, Piazza Leonardo da Vinci 32, 20133 Milano, Italy

Available online 31 January 2014

1. Introduction

The use of externally bonded Fiber Reinforced Polymer (FRP) wraps or strips both for structural strengthening and for seismic retrofitting on RC structures is nowadays widely adopted. FRP strengthening systems are very competitive when compared with traditional techniques, such as steel jacketing and plate bonding, or external prestressing. Bonding steel plates to the tension zones of beams is an effective flexural strengthening technique, but corrosion of the steel plates may occur. Besides, steel plates length and heavy weight may result in the need for joints and scaffolding. External prestressing is another technique used to strengthen concrete structures. Bars or strands are located on the external surface of the member to be strengthened. The method is effective, but requires sufficient strength in the existing concrete to transfer the stress and exposed anchorages need to be protected against corrosion and vandalism.

1.1. Problem statement

FRPs' offer extremely high mechanical and chemical characteristics. In particular, the application of FRP reinforcement increases the local stiffness, flexural and shear capacity of the strengthened member and column confinement. Besides, the fiber wraps block the intrusion of substances from the surrounding environment that might cause deterioration. Several advantages result from FRPs' low specific weight, such as minimization of the dead weight added to the structure, low transportation and labour costs. FRPs' very small thickness produces an irrelevant section enlargement or height decrease below the strengthened member, allowing crossing and overlapping of the strips and providing aesthetical solutions. Nonetheless, one of the major points of concern in the use of FRPs for structural retrofitting of concrete elements is related to surface preparation [1] and to the durability of the bond under both environmental actions (harsh environments) [2] and mechanical loading (fatigue) [3]. Besides, quality control is crucial to the successful application of FRP retrofit systems and the quality control process should start before the system is installed and should continue through installation.

1.2. Scope of the research

In this study the end peeling failure mode is taken into account. The failure mechanism concerns the in-plane shear fracture (Mode II) and its onset is close to the FRP end and propagates inward along the concrete member. In this work first an enlarged database is considered adding to push–pull debonding tests from the

* Corresponding author. Tel.: +39 0223994280.

E-mail addresses: pierluigi.colombi@polimi.it (P. Colombi), giulia.fava@polimi.it (G. Fava), carlo.poggi@polimi.it (C. Poggi).

literature push–pull debonding tests from the authors. The authors' tests were performed with both wraps and strips of different length. More precisely, 13 tests with wraps reinforcement and 17 tests with strips reinforcement were performed. The fracture energy law is then discussed and the enlarged experimental database is used to perform a refined and reliable estimation of the relevant experimental parameters. Calibrations are performed separately for wraps and strips using two different statistical models in order to appreciate the influence of the reinforcement type on the debonding load.

1.3. Previous studies

Different test set-ups were proposed in the literature to investigate the end debonding of FRP reinforcements on concrete members [4–7]. Experimental studies and numerical analyses [4,5] demonstrated that the test setup may strongly influence the debonding strength. Even though a standard procedure to analyze end debonding has not been defined yet, from an experimental point of view push–pull test setup [6,7] is easy to prepare and provides an acceptable repeatability (see Fig. 1). In such test setup, the concrete member is pushed by a compressive load while the FRP reinforcement is pulled by a tensile load (push–pull loading scheme). Due to the above reasons, shear tests are commonly used for their simplicity but there are several challenges (specimen preparation, loading alignment, presence of out of plane displacement etc.) that may lead to a certain variability of the experimental results and eventually to the scattering of the parameters related to the mode II interfacial fracture energy.

On fracture mechanics basis, theoretical models have been developed to estimate the end-debonding load on concrete elements strengthened by using FRP reinforcements [8-19]. The fracture energy concept is generally introduced to evaluate the debonding load. Debonding strength is usually considered to be a function of strength, width and surface treatment of the concrete member and of the reinforcement stiffness, width and the bond length. On the other hand, all the models based on fracture mechanics require the use of proper semi-empirical coefficients. These coefficients have to be evaluated on the basis of a statistical relevant number of consistent debonding tests.

2. Experimental program

A series of push–pull debonding tests on CFRP strips (17) and wraps (13) bonded to concrete blocks (see Fig. 2) were performed.

Concrete blocks ($150 \times 150 \times 600\ mm^3$) were fabricated. Two opposite surfaces of the concrete blocks were sandblasted until aggregates were visible to remove the top layer of mortar. CFRP reinforcement was bonded to the concrete block on opposite sides using an epoxy resin. For the CFRP strips the adhesive was evenly distributed on the adherents paying attention to avoid air bubbles and the CFRP reinforcement was pressed on the concrete surface.

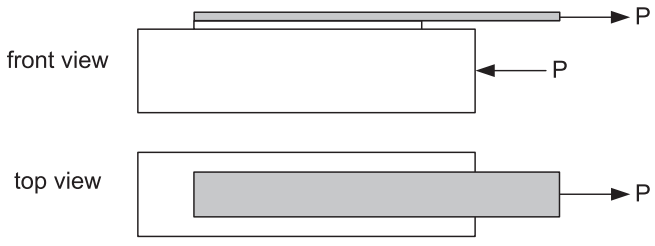

Fig. 1. The push–pull loading scheme.

For the CFRP wraps the adhesive was firstly distributed on concrete then the reinforcement was laid on the adhesive layer and finally the CFRP wrap was impregnated and pressed.

For both CFRP strips and wraps, the Young's modulus E_f was measured testing several specimens accordingly to the ASTM D3039 [20]. The composite thickness (t_f), Young's modulus (E_f), width (b_f) and length (l_{FRP}) for CFRP strips are reported in Table 1.

For the unidirectional CFRP strips, on the basis of the ISO 1172 Standard [21], a fiber volumetric content of at least 74% was measured. As reported in the technical datasheet the nominal fiber volumetric content should be greater than 70% [22]. The CFRP wraps consisted of one layer of unidirectional textile, fiber volumetric content between 27% and 30% were measured. The Young's modulus was measured referring to the fibers, testing several laminated specimens made of three CFRP wraps. CFRP reinforcements were bonded to each concrete block on opposite sides using a thixotropic bi-component epoxy resin.

Tests were performed using a mechanical testing machine with a load bearing capacity of 1000 kN (see Fig. 3a). A supporting frame consisting of four *L* profiles and two threaded tie-rods were used to correctly position the specimen in the testing rig and to avoid possible misalignments of the applied load (see Fig. 3b). The specimen was also restrained to prevent horizontal displacements. Steel plates were used to connect the CFRP strips to a 100 kN loading cell (see Fig. 3c). For the CFRP wraps, anchorages were prepared [18], inserting the CFRP between two GFRP tabs and then the system was connected to the load cell by bolted steel plates (see Fig. 3d).

Attention was given to the alignment of the CFRP reinforcement in the specimen with the applied force. In fact, when the force is not perfectly aligned, a flexural moment may generate peeling stresses and then premature debonding. For each specimen the failure load are reported in Table 1. A typical fracture surface is shown in Fig. 4, and the main types of collapse can be recognized, i.e. failure at the aggregate level (A); at the cement/aggregate interface (B); at the adhesive/FRP interface (C) and due to absence of binder (D).

After the debonding tests, four cores (75 mm by 150 mm) were obtained from each concrete block and, according to [23], compressive [24] and tensile splitting [25] tests were performed to measure the concrete strength. The mean compressive (f_{cm}) and tensile (f_{ctm}) concrete strength are reported in Table 1, for each set of specimens.

3. FRP end-debonding strength model

Theoretical studies on bond strength models have been carried out both considering single or double shear tests on FRP reinforced concrete blocks [4–7]. From an experimental point of view, pull–push joints (see Fig. 1) provide more conservative results in terms of load-carrying capacity [10,18].

In order to analyze the bond between FRP and concrete, a bond-slip relationship between interfacial shear stress τ and the corresponding adherents slip δ and fracture energy Γ_F of the interface law is required. The τ–δ relationship is typically nonlinear with a descending branch [15,17]. Nonetheless, bilinear local bond-slip models provide a close representation of the bond-slip behavior of FRP-to-concrete interfaces [10–12,14,18]. As shown in Fig. 5, the bilinear shear stress-slip relationship consists of an initial elastic ascending branch (up to $\tau_{f,\max}$ and δ_f), followed by a linear descending branch till an ultimate slip $\delta_{f,\max}$ is reached, corresponding to a full reinforcement debond. When the slip value exceeds $\delta_{f,\max}$, the shear stress value is equal to zero and an interfacial macrocrack is observed.

The selection of a simple bond-slip law as the bilinear one is considered to be reasonable and widely adopted in codes. As an example, in [15], the bilinear model is shown to produce an

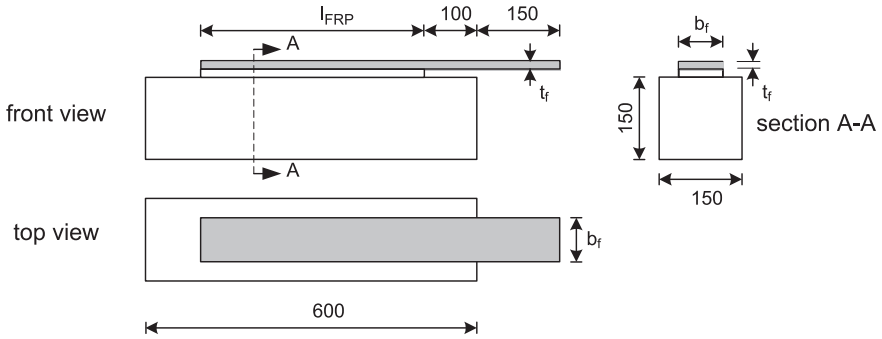

Fig. 2. Specimens' geometry (see Table 1 for details).

Table 1
Experimental database from the current experimental program.

Spec.	Reinf	f_{cm} (MPa)	f_{ctm} (MPa)	t_f (mm)	E_f (MPa)	b_f (mm)	l_{FRP} (mm)	F_{max} (kN)	k_b (–)	Γ_f (N/mm)	k_G (–)
P18A	strip	25.0	2.6	1.20	176,560	80	400	42.675	1.00	0.672	1.637
P20A	strip	25.0	2.6	1.20	176,560	80	400	36.833	1.00	0.500	1.832
P18B	strip	25.0	2.6	1.20	176,560	80	100	30.788	1.00	0.350	0.820
P20B	strip	25.0	2.6	1.20	176,560	80	100	30.018	1.00	0.332	0.781
P15A	wrap	25.0	2.6	0.22	409,289	80	400	27.590	1.00	0.660	1.665
P19A	wrap	25.0	2.6	0.22	409,289	80	400	29.185	1.00	0.739	1.240
P15B	wrap	25.0	2.6	0.22	409,289	80	100	19.519	1.00	0.331	0.867
P19B	wrap	25.0	2.6	0.22	409,289	80	100	19.052	1.00	0.315	0.824
V7A	strip	26.0	3.0	1.20	180,000	80	400	35.013	1.00	0.443	1.011
V8A	strip	26.0	3.0	1.20	180,000	80	400	29.150	1.00	0.307	0.701
V11A	strip	26.0	3.0	1.20	180,000	80	400	32.769	1.00	0.388	0.885
V7B	strip	26.0	3.0	1.20	180,000	80	100	26.810	1.00	0.260	0.593
V8B	strip	26.0	3.0	1.20	180,000	80	100	32.805	1.00	0.389	0.887
V11B	strip	26.0	3.0	1.20	180,000	80	100	32.298	1.00	0.377	0.860
V24A	wrap	26.0	3.0	0.16	239,641	100	400	25.393	1.00	0.841	1.917
V25A	wrap	26.0	3.0	0.16	239,641	100	400	24.889	1.00	0.808	1.842
V26A	wrap	26.0	3.0	0.16	239,641	100	400	24.420	1.00	0.778	1.773
V24B	wrap	26.0	3.0	0.16	239,641	100	100	20.797	1.00	0.564	1.286
V25B	wrap	26.0	3.0	0.16	239,641	100	100	23.102	1.00	0.696	1.587
V26B	wrap	26.0	3.0	0.16	239,641	100	100	22.112	1.00	0.638	1.454
S1A	strip	58.0	4.1	1.20	165,000	80	500	38.490	1.00	0.585	0.758
S1B	strip	58.0	4.1	1.20	165,000	80	500	34.890	1.00	0.480	0.623
S2A	strip	58.0	4.1	1.20	165,000	80	500	38.070	1.00	0.572	0.742
S2B	strip	58.0	4.1	1.20	165,000	80	500	33.820	1.00	0.451	0.585
S3A	strip	15.2	1.8	1.20	165,000	50	500	21.964	1.12	0.487	1.647
S3B	strip	15.2	1.8	1.20	165,000	50	500	23.400	1.12	0.553	1.869
S4A	strip	15.2	1.8	1.20	165,000	50	500	20.313	1.12	0.417	1.409
S4B	wrap	15.2	1.8	0.22	239,050	80	500	21.445	1.00	0.683	2.582
S5A	wrap	15.2	1.8	0.22	239,050	80	500	21.049	1.00	0.658	2.487
S5B	wrap	15.2	1.8	0.22	239,050	80	500	19.850	1.00	0.585	2.212

f_{cm} = concrete compressive strength.
f_{ctm} = concrete tensile strength.
t_f = reinforcement thickness.
E_f = reinforcement Young's modulus.
b_f = reinforcement bond width.
l_{FRP} = reinforcement bond length.
F_{max} = debonding force.
k_b = geometrical factor (see Eq. (4)).
Γ_f = fracture energy (see Eq. (13)).
k_G = fracture energy coefficient (see Eq. (14)).

estimation of the debonding force which is in good agreement with experimental results.

From [14], the maximum transferable load F_{max} for the push–pull loading scheme depends on fracture energy Γ_F and on the FRP mechanical and geometrical properties:

$$F_{max} = b_f \sqrt{2 \cdot \Gamma_f \cdot E_f \cdot t_f} \tag{1}$$

where b_f and t_f are the FRP width and thickness, respectively, while E_f are Γ_f the elastic modulus and the mode II interfacial fracture energy, respectively. Note that the fracture energy Γ_f, physically represents the area under the bond-slips law:

$$\Gamma_f = \int_0^\infty \tau(\delta(x)) \cdot dx = \frac{1}{2} \tau_{f,max} \cdot \delta_{f,max} \tag{2}$$

When a plate is bonded to a concrete specimen and is subject to shear test, mode II shear failure usually occurs. Only a small layer of concrete close to interface is subjected to very high shear stresses and the fracture mode requires that the fracture propagates along it. Since the concrete strength is lower than the adhesive ones, final shear cracks typically occur few millimeters below the

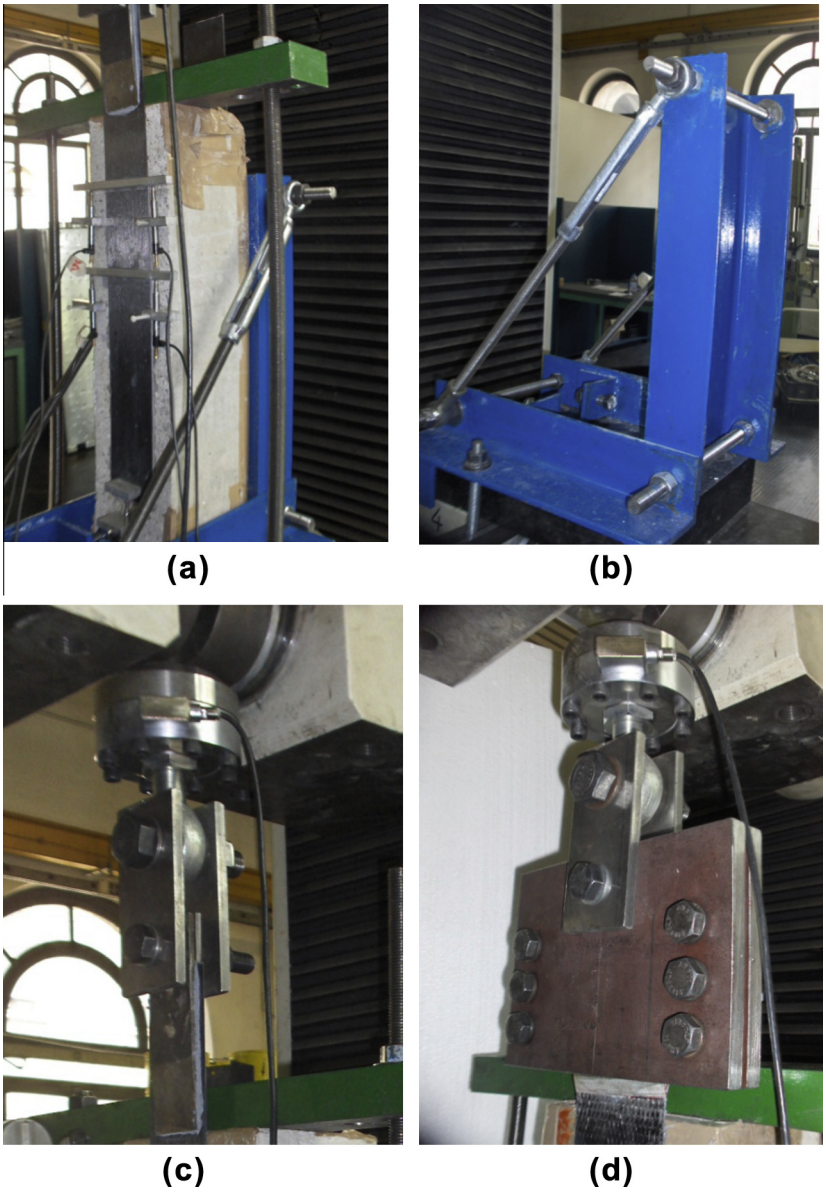

Fig. 3. Experimental set-up: (a) testing machine, (b) testing rig, (c) anchorage system for strips and (d) anchorage system for wraps.

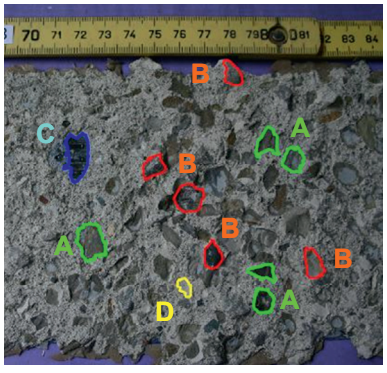

Fig. 4. Typical fracture surface.

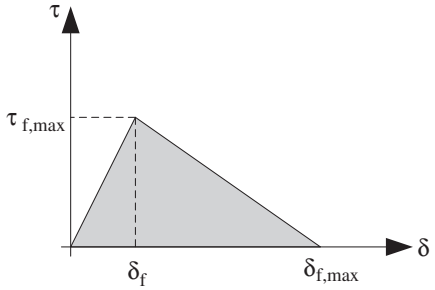

Fig. 5. Bilinear bond-slip model.

adhesive-concrete interface. The interfacial mode II fracture energy is much higher than mode I fracture energy of concrete, as confirmed by several experimental studies [15].

Based on some design recommendations on the use of FRP for strengthening existing concrete structures [26,27], the bond-slip behavior of the adhesive joint between FRP and concrete, in terms of average shear stress τ versus adherents slip δ, is idealized by means of a bilinear function (see Fig. 5). Following the

Mohr–Coulomb failure criterion [28] and considering that, as stated before, debonding generally occurs in concrete, the maximum shear stress is generally expressed as a function of the concrete strength [27]:

$$\tau_{f,\max} = \frac{1}{2} k_b \sqrt{f_{cm} f_{ctm}} \tag{3}$$

where f_{cm} and f_{ctm} represent the mean concrete strength in compression and in tension, respectively, while k_b ($k_b \geqslant 1$) is a geometrical factor [4] describing the effect of the ratio between the reinforcement width b_f and the concrete width b_c:

$$k_b = \sqrt{\left(2 - \frac{b_f}{b_c}\right) \Big/ \left(1 + \frac{b_f}{b_c}\right)} \geqslant 1 \quad \left(\frac{b_f}{b_c} \geqslant 0.25\right) \tag{4}$$

Eq. (4) is effective for $b_f/b_c \geqslant 0.25$ while for $b_f/b_c < 0.25$ the value corresponding to $b_f/b_c = 0.25$ is used (see Fig. 6). The width ratio between the FRP and the concrete substrate plays an important role on the bond strength. When the FRP width is smaller than that of the concrete element, non-uniform stress distribution across the concrete width b_c and higher adhesive shear stresses at failure are observed during the load transfer due to influence of the concrete outside the bond area. The coefficient k_b also represents the effects of the reinforcement transversal contraction. If the FRP width is comparable to the concrete width a biaxial stress state will take place in the reinforcement while if the FRP width is significantly smaller than the substrate width the stress state will be uniaxial.

The fracture energy of interface law is then expressed as (see Eqs. (2) and (3)):

$$\Gamma_f = \frac{1}{4} k_G \cdot k_b \cdot \sqrt{f_{cm} f_{ctm}} \cdot \delta_{f,\max} \tag{5}$$

where k_G is the fracture energy coefficient to calibrate experimentally. This coefficient considers all the parameters that are not included in the bond strength model. Note that the fracture energy in Eq. (5) is expressed as a function of the concrete tensile and compressive strength properties and is written in a similar way to that used for failure mode I in concrete. This agrees both with fracture energy evaluation using nonlinear fracture mechanics [29,30] and with experimental observations [31]. The final expression of the debonding load $F_{\max}$ is then (see Eq. (1)):

$$F_{\max} = b_f \cdot \beta_1 \cdot \sqrt{2 \cdot \Gamma_f \cdot E_f \cdot t_f} \tag{6}$$

where β_1 is the reduction factor [28] which takes into account the influence of the bond length, l_b (see Fig. 7):

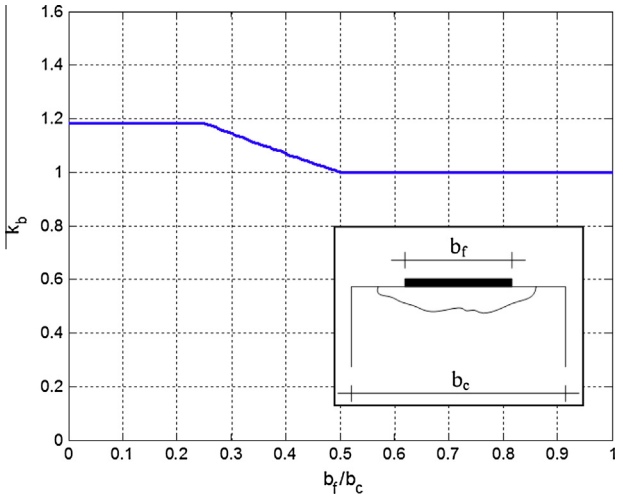

Fig. 6. Correction factor k_b.

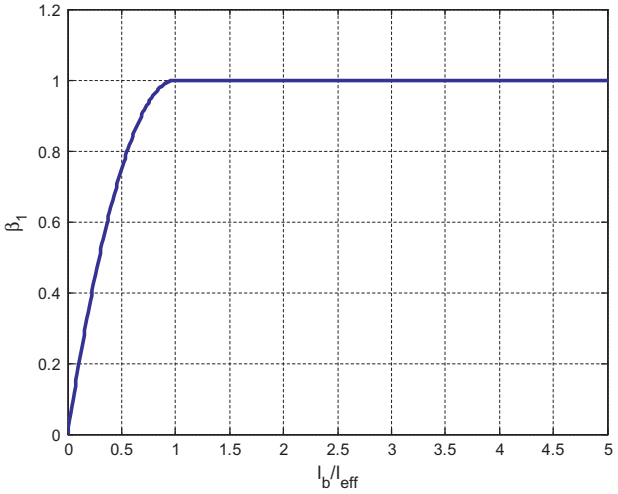

Fig. 7. Correction factor β_1.

$$\beta_1 = \frac{l_b}{l_{eff}} \cdot \left(2 - \frac{l_b}{l_{eff}}\right) \tag{7}$$

and l_{eff} is the effective bond length:

$$l_{eff} = \sqrt{\frac{E_f t_f}{2 f_{ctm}}} \tag{8}$$

Eq. (6) is the model prediction for the failure load and it will be used in the following together with Eq. (5) to calibrate the model parameters. As the failure load is known (see Table 1) from the experimental tests, from Eq. (6) the fracture energy parameters Γ_f is first evaluated and reported in Table 1. Finally from Eq. (5) the fracture energy coefficient k_G is determined and again stated in Table 1. This procedure is illustrated in the next section.

3.1. Further considerations on the debonding strength model

In this section, further considerations on the design formula for the specific fracture energy and for the maximum load transferred between FRP and concrete are presented.

At first, the values of the maximum shear stress $\tau_{f,\max}$ and of the maximum slip $\delta_{f,\max}$ need to be evaluated in order to compute the fracture energy Γ_f (see Eq. (2)). Chen and Teng [4] suggested a maximum slip value at failure $\delta_{f,\max}$ of 0.2 mm for FRP-to-concrete bonded joints. The Mohr–Coulomb failure criterion is used to determine the value of $\tau_{f,\max}$ [28]. In the plane (σ, τ), the Mohr–Coulomb limit lines are tangent to both the limit Mohr's circle for pure tension and pure compression (see Fig. 8). Mohr's circles tangent to the Mohr–Coulomb critical lines represent then a failure condition.

The parameters of the Mohr–Coulomb critical lines can be expressed, by simple geometric considerations, as function of the mean compression and tensile strength:

$$\overline{OA} = \frac{f_{cm}}{2\sqrt{k}}, \qquad tg\varphi = \frac{k-1}{2\sqrt{k}} \tag{9}$$

where $k = f_{cm}/f_{ctm}$. In a pull–push testing configuration, plane stress condition is present in the concrete block close to the adhesive joint. Moreover, the peel stress is generally neglected in the literature and then the stress state is the one reported in Fig. 8.

In Fig. 8 the corresponding limit Mohr's circle is also reported. Two limit situations are clearly identified:

- the pure compression limit Mohr's circle;
- the pure tension limit Mohr's circle;

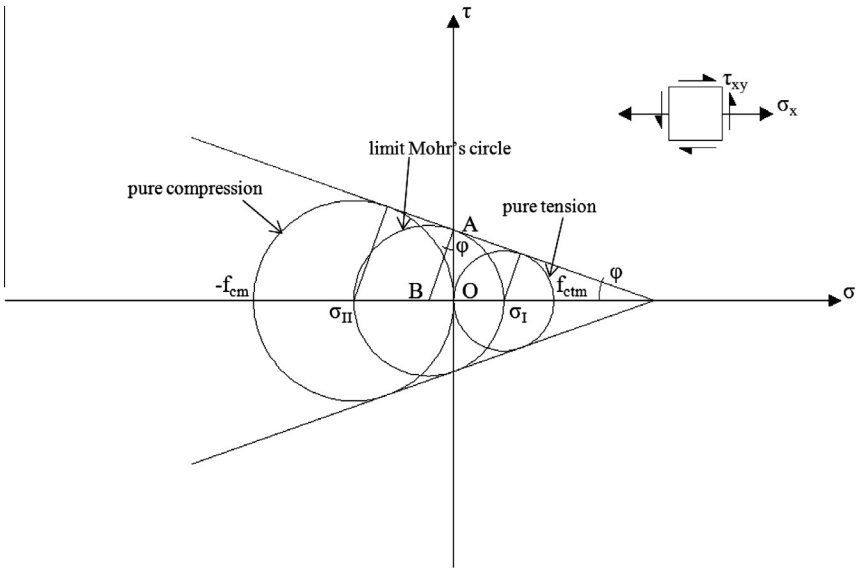

Fig. 8. Limit Mohr's circle for the push–pull test configuration.

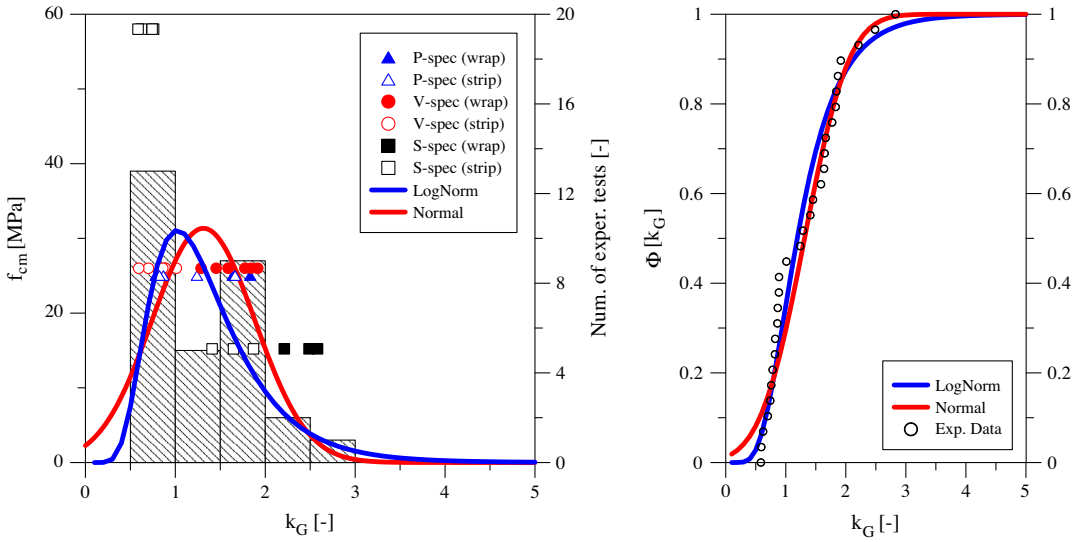

Fig. 9. Statistical analysis of tests results from the current experimental program.

Between these two limiting situations a choice should be made for the limit Mohr's circle corresponding to the push–pull testing configuration in order to evaluate the critical shear stress $\tau_{f,\max}$. In some design recommendations [26,27] it is assumed that the critical Mohr's circle is tangent in A [28] to the Mohr–Coulomb limit lines (see Fig. 8).

The parameters of this critical Mohr's circle are:

$$\begin{aligned} \overline{OA} &= \frac{f_{cm}}{2\sqrt{k}} \\ \overline{OB} &= \overline{OA}\cdot tg\varphi = -f_{cm}\cdot\frac{k-1}{4k} \\ \overline{AB} &= \sqrt{\overline{OA}^2+\overline{OB}^2} = f_{cm}\cdot\frac{k+1}{4k} \\ \sigma_I &= \overline{OB}+\overline{AB} = \frac{f_{ctm}}{2}; \qquad \sigma_{II} = \overline{OB}-\overline{AB} = -\frac{f_{cm}}{2} \end{aligned} \tag{10}$$

From Eq. (10) one has $|\sigma_I| \neq |\sigma_{II}|$ and:

$$\left|\frac{\sigma_{II}}{\sigma_I}\right| = \frac{f_{cm}}{f_{ctm}} \tag{11}$$

From this point of view, it is also interesting to observe that finite elements results of pull–push debonding tests provided in [32] show that the ratio $|\sigma_I/\sigma_{II}|$ is almost 9 and approximately equal to the ratio f_{cm}/f_{ctm}. It is also noted a higher shear and normal stress concentration in the concrete substrate, corresponding to the reinforcement debonding.

The critical shear stress $\tau_{f,\max}$ may be expressed as a function of the compressive strength f_{cm} and of the tensile strength f_{ctm}:

$$\tau_{f,\max} = \overline{OA} = f_{ctm}\frac{\sqrt{k}}{2} = \frac{1}{2}\sqrt{f_{cm}f_{ctm}} \tag{12}$$

Moreover, concrete composition, specifically the porosity and coarse aggregate size of the concrete, affects the stress transfer region depth and then the deformability of the concrete layer. It is usually implicitly included in the bond-slip interface law.

Finally note that for large k, the critical shear stress is significantly larger than the concrete tensile strength and the fracture energy Γ_f is exactly given by Eq. (5).

Then, based on a statistical analysis over the experimental results, the mean and characteristic values for the coefficient k_G are

Table 2
Experimental enlarged database (CFRP wraps).

Spec.	Reinf	f_{cm} (MPa)	f_{ctm} (MPa)	t_f (mm)	E_f (MPa)	b_f (mm)	b_c (mm)	L_{frp} (mm)	F_{max} (kN)	k_b (−)	Γ_f (N/mm)	k_G (−)
By authors	P15A	25.03	2.60	0.220	409,289	80	150	400	27.59	1.000	0.660	1.637
	P19A	25.03	2.60	0.220	409,289	80	150	400	29.19	1.000	0.739	1.832
	P15B	25.03	2.60	0.220	409,289	80	150	100	19.52	1.000	0.331	0.820
	P19B	25.03	2.60	0.220	409,289	80	150	100	19.05	1.000	0.315	0.781
	V24A	26.00	2.96	0.160	239,641	100	150	400	25.39	1.000	0.841	1.917
	V25A	26.00	2.96	0.160	239,641	100	150	400	24.89	1.000	0.808	1.842
	V26A	26.00	2.96	0.160	239,641	100	150	400	24.42	1.000	0.778	1.773
	V24B	26.00	2.96	0.160	239,641	100	150	100	20.80	1.000	0.564	1.286
	V25B	26.00	2.96	0.160	239,641	100	150	100	23.10	1.000	0.696	1.587
	V26B	26.00	2.96	0.160	239,641	100	150	100	22.11	1.000	0.638	1.454
	S4B	15.21	1.84	0.220	239,050	80	150	500	21.44	1.000	1.147	2.582
	S5A	15.21	1.84	0.220	239,050	80	150	500	21.05	1.000	1.014	2.487
	S5B	15.21	1.84	0.220	239,050	80	150	500	19.85	1.000	0.907	2.212
Takeo et al. [33]	1–11	36.56	2.86	0.167	230,000	40	100	100	8.75	1.069	0.623	1.140
	1–12	33.75	2.74	0.167	230,000	40	100	100	8.85	1.069	0.637	1.240
	1–21	36.56	2.86	0.167	230,000	40	100	200	9.30	1.069	0.704	1.287
	1–22	33.75	2.74	0.167	230,000	40	100	200	8.50	1.069	0.588	1.144
	1–31	36.56	2.86	0.167	230,000	40	100	300	9.30	1.069	0.704	1.287
	1–32	33.75	2.74	0.167	230,000	40	100	300	8.30	1.069	0.560	1.090
	1–41	36.56	2.86	0.167	230,000	40	100	500	8.05	1.069	0.527	0.965
	1–42	36.56	2.86	0.167	230,000	40	100	500	8.05	1.069	0.527	0.965
	1–51	33.50	2.73	0.167	230,000	40	100	500	8.45	1.069	0.581	1.136
	1–52	33.50	2.73	0.167	230,000	40	100	500	7.30	1.069	0.434	0.848
	2–11	31.63	2.64	0.167	230,000	40	100	100	8.75	1.069	0.623	1.275
	2–12	31.63	2.64	0.167	230,000	40	100	100	8.85	1.069	0.637	1.305
	2–13	33.13	2.71	0.167	230,000	40	100	100	7.75	1.069	0.489	0.965
	2–14	33.13	2.71	0.167	230,000	40	100	100	7.65	1.069	0.476	0.940
	2–15	30.88	2.61	0.167	230,000	40	100	100	9.00	1.069	0.659	1.373
	2–51	31.13	2.71	0.167	230,000	40	100	100	9.85	1.069	0.789	1.608
	2–52	31.13	2.71	0.167	230,000	40	100	100	9.50	1.069	0.734	1.496
	2–61	31.13	2.71	0.167	230,000	40	100	100	8.80	1.069	0.630	1.283
	2–62	30.13	2.71	0.167	230,000	40	100	100	9.25	1.069	0.696	1.441
	2–71	30.13	2.71	0.167	230,000	40	100	100	7.65	1.069	0.476	0.986
	2–72	33.13	2.71	0.167	230,000	40	100	100	6.80	1.069	0.376	0.743
	2–81	33.25	3.87	0.167	230,000	40	100	100	7.75	1.069	0.489	0.806
	2–82	33.25	3.87	0.167	230,000	40	100	100	8.05	1.069	0.527	0.870
	2–91	33.88	2.61	0.167	230,000	40	100	100	6.75	1.069	0.371	0.737
	2–92	33.88	2.61	0.167	230,000	40	100	100	6.80	1.069	0.376	0.748
	2–101	33.63	2.64	0.111	230,000	40	100	100	7.70	1.069	0.726	1.441
	2–102	63.13	2.71	0.111	230,000	40	100	100	6.95	1.069	0.591	0.846
Yao et al. [5]	I-6	23.00	1.82	0.165	256,000	25	150	115	5.96	1.254	0.673	1.657
	I-7	23.00	1.82	0.165	256,000	25	150	145	5.95	1.254	0.671	1.651
	I-8	23.00	1.82	0.165	256,000	25	150	190	6.68	1.254	0.845	2.081
	I-9	23.00	1.82	0.165	256,000	25	150	190	6.35	1.254	0.764	1.881
	I-14	23.00	1.82	0.165	256,000	25	150	115	6.19	1.254	0.726	1.787
	I-15	23.00	1.82	0.165	256,000	25	150	145	6.27	1.254	0.745	1.834
	I-16	23.00	1.82	0.165	256,000	25	150	190	7.03	1.254	0.936	2.305
	II-5	24.06	1.91	0.165	256,000	25	150	190	7.07	1.254	0.947	2.228
	III-1	28.47	2.25	0.165	256,000	25	150	100	5.94	1.254	0.668	1.334
	III-2	28.47	2.25	0.165	256,000	50	150	100	11.66	1.118	0.644	1.440
	III-3	28.47	2.25	0.165	256,000	75	150	100	14.63	1.000	0.450	1.127
	III-4	28.47	2.25	0.165	256,000	100	150	100	19.07	1.000	0.430	1.077
	III-5	27.10	2.14	0.165	256,000	85	100	100	15.08	1.000	0.373	0.978
	III-6	27.10	2.14	0.165	256,000	100	100	100	15.75	1.000	0.294	0.771
	VI-3	21.90	1.73	0.165	256,000	25	150	145	5.76	1.254	0.628	1.627
	VI-4	21.90	1.73	0.165	256,000	25	150	145	5.73	1.254	0.622	1.610
	VI-5	21.90	1.73	0.165	256,000	25	150	190	5.56	1.254	0.585	1.516
	VI-6	21.90	1.73	0.165	256,000	25	150	190	5.58	1.254	0.590	1.527
	VI-7	21.90	1.73	0.165	256,000	25	150	240	5.91	1.254	0.662	1.713
	VI-8	21.90	1.73	0.165	256,000	25	150	240	5.05	1.254	0.483	1.250
	VII-3	24.90	1.98	0.165	256,000	25	150	145	7.33	1.254	1.018	2.315
	VII-4	24.90	1.98	0.165	256,000	25	150	145	6.49	1.254	0.798	1.815
	VII-5	24.90	1.98	0.165	256,000	25	150	190	7.07	1.254	0.947	2.153
	VII-6	24.90	1.98	0.165	256,000	25	150	190	7.44	1.254	1.048	2.385
	VII-7	24.90	1.98	0.165	256,000	25	150	240	7.16	1.254	0.971	2.209
	VII-8	24.90	1.98	0.165	256,000	25	150	240	6.24	1.254	0.737	1.677
Fava et al. [34]	R7A	36.60	2.81	0.166	288,000	100	200	500	23.84	1.000	0.594	1.172
	R7B	36.60	2.81	0.166	288,000	100	200	500	28.77	1.000	0.866	1.707
	R8A	36.60	2.81	0.166	288,000	100	200	500	23.72	1.000	0.588	1.160
	R8B	36.60	2.81	0.166	288,000	100	200	500	25.00	1.000	0.654	1.289
	R10B	36.60	2.81	0.166	288,000	100	200	500	24.40	1.000	0.623	1.228

Table 2 (*continued*)

Spec.	Reinf	f_{cm} (MPa)	f_{ctm} (MPa)	t_f (mm)	E_f (MPa)	b_f (mm)	b_c (mm)	L_{frp} (mm)	F_{max} (kN)	k_b (–)	Γ_f (N/mm)	k_G (–)
Ceroni and Pecce [35]	C150_100_1	34.27	2.65	0.165	230,000	100	150	150	18.97	1.000	0.474	0.995
	C150_100_2	34.27	2.65	0.165	230,000	100	150	150	16.51	1.000	0.359	0.754
	C150_100_3	34.27	2.65	0.165	230,000	100	150	150	14.26	1.000	0.268	0.562
	C150_100_4	34.27	2.65	0.165	230,000	100	150	150	15.10	1.000	0.300	0.630
	C150_100_2L_1	34.27	2.65	0.165	230,000	100	150	150	20.12	1.000	0.533	1.119
	C150_100_2L_2	34.27	2.65	0.165	230,000	100	150	150	19.87	1.000	0.520	1.092
	C100_100_1	34.27	2.65	0.165	230,000	100	150	100	13.63	1.000	0.245	0.514
	C100_100_2	34.27	2.65	0.165	230,000	100	150	100	13.36	1.000	0.235	0.494
	C150_50_1	34.27	2.65	0.165	230,000	50	150	150	9.80	1.118	0.506	0.950
	C150_50_2	34.27	2.65	0.165	230,000	50	150	150	6.00	1.118	0.190	0.356
	C150_50_3	34.27	2.65	0.165	230,000	50	150	150	7.00	1.118	0.258	0.485
	C150_50_2L_1	34.27	2.65	0.165	230,000	50	150	150	11.44	1.118	0.690	1.295
	C150_50_2L_2	34.27	2.65	0.165	230,000	50	150	150	9.97	1.118	0.524	0.983
	C150_50_2L_3	34.27	2.65	0.165	230,000	50	150	150	10.04	1.118	0.531	0.997
	C150_25_1	34.27	2.65	0.165	230,000	25	150	150	6.00	1.254	0.759	1.270
	C150_25_2	34.27	2.65	0.165	230,000	25	150	150	3.70	1.254	0.289	0.483
	C150_25_3	34.27	2.65	0.165	230,000	25	150	150	5.80	1.254	0.709	1.187
	C150_75_1	34.27	2.65	0.165	230,000	75	150	150	14.40	1.000	0.486	1.019
	C150_75_2	34.27	2.65	0.165	230,000	75	150	150	12.96	1.000	0.393	0.826
Bilotta et al. [7]	V18A	26.00	2.96	0.160	241,000	100	150	400	24.00	1.000	0.747	1.703
	V19A	26.00	2.96	0.160	241,000	100	150	400	24.96	1.000	0.808	1.842
	V20A	26.00	2.96	0.160	241,000	100	150	400	23.65	1.000	0.725	1.653
	V18B	26.00	2.96	0.160	241,000	100	150	100	21.84	1.000	0.618	1.410
	V19B	26.00	2.96	0.160	241,000	100	150	100	21.49	1.000	0.599	1.365
	V20B	26.00	2.96	0.160	241,000	100	150	100	21.91	1.000	0.622	1.419
	SM1	23.82	2.48	0.166	230,000	100	150	400	21.41	1.000	0.600	1.561
	SM2	23.82	2.48	0.166	230,000	100	150	400	21.81	1.000	0.623	1.620
	SM3	23.82	2.48	0.166	230,000	100	150	400	21.24	1.000	0.591	1.536
	SC4	23.82	2.48	0.166	230,000	100	150	400	21.69	1.000	0.616	1.602
	SC5	23.82	2.48	0.166	230,000	100	150	400	20.74	1.000	0.563	1.465
	SC6	23.82	2.48	0.166	230,000	100	150	400	22.11	1.000	0.640	1.665
	SM7	21.46	2.32	0.166	230,000	100	150	100	19.37	1.000	0.491	1.394
	SM8	21.46	2.32	0.166	230,000	100	150	100	20.37	1.000	0.543	1.541
	SM9	21.46	2.32	0.166	230,000	100	150	100	22.58	1.000	0.668	1.894
	SM13	21.46	2.32	0.166	230,000	100	150	100	16.85	1.000	0.372	1.055
	SM14	21.46	2.32	0.166	230,000	100	150	100	21.20	1.000	0.589	1.669
	SM15	21.46	2.32	0.166	230,000	100	150	100	19.03	1.000	0.474	1.345

f_{cm} = concrete compressive strength.
f_{ctm} = concrete tensile strength.
t_f = reinforcement thickness.
E_f = reinforcement Young's modulus.
b_f = reinforcement bond width.
l_{FRP} = reinforcement bond length.
F_{max} = debonding force.
k_b = geometrical factor (see Eq. (4)).
Γ_f = fracture energy (see Eq. (13)).
k_G = fracture energy coefficient (see Eq. (14)).

experimentally determined for reinforcements consisting of both CFRP wraps and CFRP strips. At first, (see Eq. (6)), the fracture energy is evaluated as:

$$\Gamma_f = \frac{F_{\max}^2}{\beta_1^2 \cdot b_f^2 \cdot (2 \cdot E_f \cdot t_f)} \tag{13}$$

and it is reported in Table 1 together with the coefficient k_b. In detail, when CFRP wraps are used to strengthen the concrete element, E_f and t_f are the elastic modulus and the equivalent thickness referred to the fibers while for CFRP strips E_f and t_f are the elastic modulus and the real thickness referred to the composite material. From Eq. (5) with $\delta_{f,\max}$ = 0.2 mm and Eq. (12), the mode II interfacial fracture energy parameter k_G is then calculated and reported in Table 1:

$$k_G = \frac{2 \cdot \Gamma_f}{k_b \cdot \delta_{f,\max} \cdot \tau_{f,\max}} = \frac{2 \cdot \Gamma_f}{k_b \cdot 0.1 \cdot \sqrt{f_{cm} f_{ctm}}} \tag{14}$$

where coefficient k_b is expressed in Eq. (4).

In Fig. 9, the experimental cumulative distribution function of k_G for FRP wraps and strips tested at Politecnico of Milan is plotted and compared to the normal and lognormal theoretical model.

4. Calibration of the theoretical model

In this section, the experimental results of 30 push–pull shear tests on CFRP wraps and strips bonded to concrete blocks performed at Politecnico di Milano on CFRP were combined to a set of data available in literature in order to get an enlarged database. A database of 119 tests results was obtained for push–pull shear tests on CFRP wraps (Table 2), while 59 experimental results were selected for push–pull shear tests on CFRP strips (Table 3).

Tables 2 and 3 report for each configuration the recorded experimental failure load $F_{\max}$, the concrete properties f_{cm} and f_{ctm}, the reinforcement type (strip or wrap), the geometry (t_f, b_f and l_{FRP}) and the mechanical property of the FRP (E_f). The fracture energy Γ_f and the fracture energy coefficient k_G were evaluated according to Eqs. (13) and (14) while k_b was computed by using Eq. (4). Experimental data for CFRP wraps reinforcement were selected from [5,7,33–35] and are reported in Table 2. For CFRP strips

Table 3
Experimental enlarged database (CFRP strips).

Spec.	Reinf	f_{cm} (MPa)	f_{ctm} (MPa)	t_f (mm)	E_f (MPa)	b_f (mm)	b_c (mm)	L_{frp} (mm)	F_{max} (kN)	k_b (–)	Γ_f (N/mm)	k_G (–)
By authors	P18A	25.03	2.60	1.2	176,560	80	150	400	42.68	1.000	0.672	1.665
	P20A	25.03	2.60	1.2	176,560	80	150	400	36.83	1.000	0.500	1.240
	P18B	25.03	2.60	1.2	176,560	80	150	100	30.79	1.000	0.350	0.867
	P20B	25.03	2.60	1.2	176,560	80	150	100	30.02	1.000	0.332	0.824
	V7A	26.00	2.96	1.2	180,000	80	150	400	35.01	1.000	0.443	1.011
	V8A	26.00	2.96	1.2	180,000	80	150	400	29.15	1.000	0.307	0.701
	V11A	26.00	2.96	1.2	180,000	80	150	400	32.77	1.000	0.388	0.885
	V7B	26.00	2.96	1.2	180,000	80	150	100	26.81	1.000	0.260	0.593
	V8B	26.00	2.96	1.2	180,000	80	150	100	32.81	1.000	0.389	0.887
	V11B	26.00	2.96	1.2	180,000	80	150	100	32.30	1.000	0.377	0.860
	S1A	58.00	4.10	1.2	165,000	80	150	500	38.49	1.000	0.585	0.758
	S1B	58.00	4.10	1.2	165,000	80	150	500	34.89	1.000	0.480	0.623
	S2A	58.00	4.10	1.2	165,000	80	150	500	38.07	1.000	0.572	0.742
	S2B	58.00	4.10	1.2	165,000	80	150	500	33.82	1.000	0.451	0.585
	S3A	15.21	1.84	1.2	165,000	50	150	500	21.96	1.118	0.487	1.647
	S3B	15.21	1.84	1.2	165,000	50	150	500	23.40	1.118	0.553	1.869
	S4A	15.21	1.84	1.2	165,000	50	150	500	20.31	1.118	0.417	1.409
Taljsten [36]	C200 50A	58.50	4.10	1.25	170,000	50	200	200	27.50	1.183	0.712	0.777
	C300 50A	62.20	4.30	1.25	170,000	50	200	300	35.10	1.183	1.160	1.198
	C400 50A	62.20	4.30	1.25	170,000	50	200	400	26.90	1.183	0.681	0.704
Mazzotti et al. [37]	MFS1	52.60	3.81	1.2	195,200	50	150	400	22.80	1.118	0.444	0.561
	MFS2	52.60	3.81	1.2	195,200	80	150	400	36.20	0.978	0.437	0.631
Fava et al. [34]	R17A	36.60	2.81	1.4	371,000	50	200	500	42.24	1.183	0.687	1.145
	R17B	36.60	2.81	1.4	371,000	50	200	500	41.56	1.183	0.665	1.109
	R18A	36.60	2.81	1.4	371,000	50	200	500	35.09	1.183	0.474	0.790
	R18B	36.60	2.81	1.4	371,000	50	200	500	33.60	1.183	0.435	0.725
	R19A	36.60	2.81	1.4	371,000	50	200	500	24.99	1.183	0.240	0.401
	R19B	36.60	2.81	1.4	371,000	50	200	500	47.83	1.183	0.881	1.468
Bilotta [38]	C-1.30 × 60–1	19.00	1.48	1.3	175,000	60	160	300	33.18	1.087	0.672	2.332
	C-1.30 × 60–2	19.00	1.48	1.3	175,000	60	160	300	29.86	1.087	0.544	1.888
	C-1.30 × 60–3	19.00	1.48	1.3	175,000	60	160	300	31.88	1.087	0.620	2.153
	C-1.60 × 100–1	19.00	1.48	1.6	109,000	100	160	300	49.41	1.000	0.700	2.640
	C-1.60 × 100–2	19.00	1.48	1.6	109,000	100	160	300	39.87	1.000	0.456	1.719
	C-1.60 × 100–3	19.00	1.48	1.6	109,000	100	160	300	47.72	1.000	0.653	2.462
	C-1.20 × 100–1	19.00	1.48	1.2	166,000	100	160	300	49.85	1.000	0.624	2.353
	C-1.20 × 100–2	19.00	1.48	1.2	166,000	100	160	300	48.05	1.000	0.580	2.186
	C-1.20 × 100–3	19.00	1.48	1.2	166,000	100	160	300	52.60	1.000	0.694	2.619
	C-1.25 × 100–1	19.00	1.48	1.25	171,000	100	160	300	41.25	1.000	0.398	1.501
	C-1.25 × 100–2	19.00	1.48	1.25	171,000	100	160	300	38.14	1.000	0.340	1.283
	C-1.25 × 100–3	19.00	1.48	1.25	171,000	100	160	300	32.68	1.000	0.250	0.942
	C-1.70 × 100–1	19.00	1.48	1.7	141,000	100	160	300	54.79	1.000	0.626	2.362
	C-1.70 × 100–2	19.00	1.48	1.7	141,000	100	160	300	51.41	1.000	0.551	2.079
	C-1.70 × 100–3	19.00	1.48	1.7	141,000	100	160	300	54.57	1.000	0.621	2.343
Bilotta et al. [7]	V1A	26.00	2.96	1.2	180,000	80	150	400	30.14	1.000	0.329	0.749
	V2A	26.00	2.96	1.2	180,000	80	150	400	33.56	1.000	0.407	0.929
	V3A	26.00	2.96	1.2	180,000	80	150	400	32.47	1.000	0.381	0.869
	V1B	26.00	2.96	1.2	180,000	80	150	100	28.33	1.000	0.290	0.662
	V2B	26.00	2.96	1.2	180,000	80	150	100	27.58	1.000	0.275	0.627
	V3B	26.00	2.96	1.2	180,000	80	150	100	30.29	1.000	0.332	0.757
	PM1	23.82	2.48	1.4	170,000	50	150	400	20.10	1.118	0.340	0.790
	PM2	23.82	2.48	1.4	170,000	50	150	400	21.78	1.118	0.399	0.927
	PM3	23.82	2.48	1.4	170,000	50	150	400	20.71	1.118	0.360	0.838
	PC4	23.82	2.48	1.4	170,000	50	150	400	21.55	1.118	0.390	0.908
	PM7	21.46	2.32	1.4	170,000	50	150	250	19.02	1.118	0.304	0.771
	PM8	21.46	2.32	1.4	170,000	50	150	250	19.86	1.118	0.331	0.841
	PM9	21.46	2.32	1.4	170,000	50	150	250	17.24	1.118	0.250	0.634
	PM13	21.46	2.32	1.4	170,000	50	150	250	19.46	1.118	0.318	0.807
	PM14	21.46	2.32	1.4	170,000	50	150	250	19.30	1.118	0.313	0.794
	PM15	21.46	2.32	1.4	170,000	50	150	250	20.74	1.118	0.361	0.917

f_{cm} = concrete compressive strength.
f_{ctm} = concrete tensile strength.
t_f = reinforcement thickness.
E_f = reinforcement Young's modulus.
b_f = reinforcement bond width.
l_{FRP} = reinforcement bond length.
F_{max} = debonding force.
k_b = geometrical factor (see Eq. (4)).
Γ_f = fracture energy (see Eq. (13)).
k_G = fracture energy coefficient (see Eq. (14)).

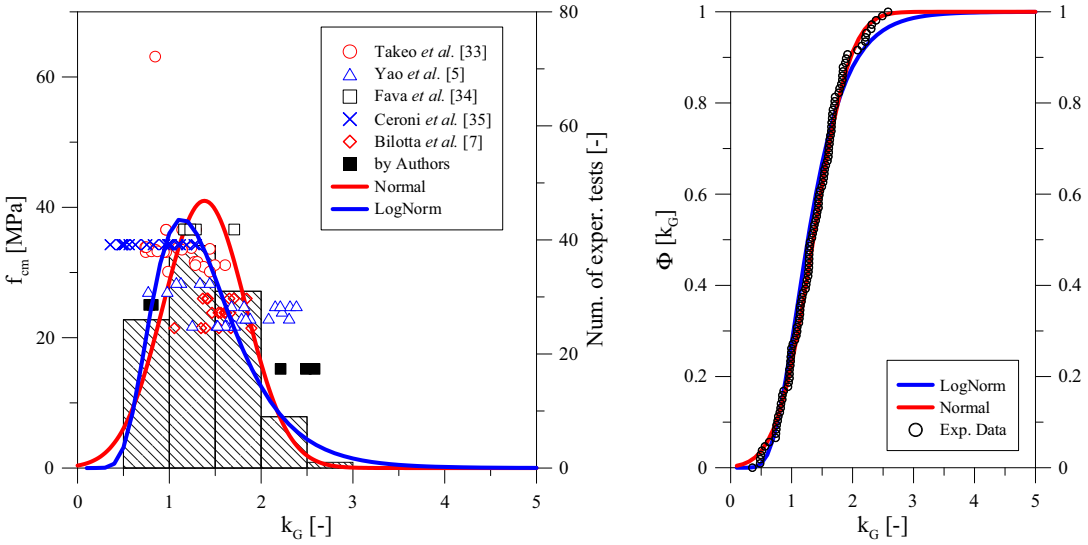

Fig. 10. Statistical analysis of tests results from the enlarged experimental database (FRP wraps reinforcement).

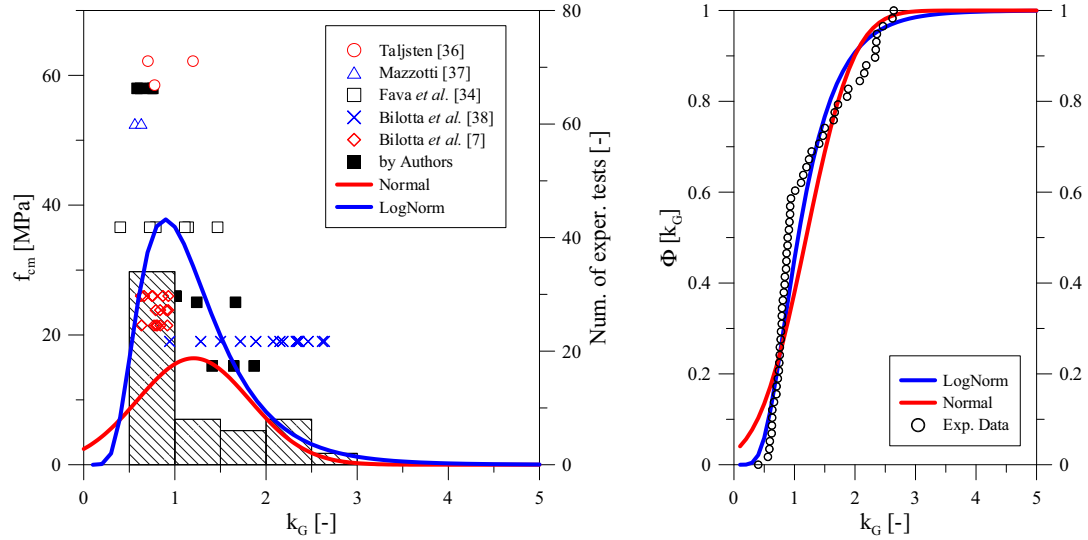

Fig. 11. Statistical analysis of tests results from the enlarged experimental database (FRP strips reinforcement).

reinforcement, experimental data were taken from [7,34,36–38] and are reported in Table 3. In general, specimens reinforced with two or more CFRP wrap layers were not considered. Only data referring to debonding failure modes were taken into account together with specimens with a CFRP reinforcement bond length greater than the effective bond length l_{eff} (see Eq. (8)).

In case of incomplete experimental data, the tensile concrete strength f_{ctm} was determined following the EC2 expressions (in MPa) [39]

$$f_{ctm} = 0.3 \cdot (f_{cm} - 8)^{2/3} \tag{15}$$

Concerning the experimental data taken from [5], among the seven different specimen sets taken into account, only specimens with no loading offset were inserted in the database of Table 2. In [34] the effect of the aggressive environment on the bond strength was investigated and two groups of specimens were subject to freeze–thaw or salt spray fog treatment, but in this work only unconditioned specimens were taken into account. In [35], different types of end anchorage devices were used to investigate the effectiveness of various techniques for anchoring the reinforcement end, but only specimens without anchoring systems were selected for the database of Table 2. Besides, the concrete compressive strength was not available and therefore was determined on the basis of a mean cubic compressive strength of 36 MPa. Finally, in [33] the bond efficiency of both FRP bars and strips was examined, but specimens reinforced with FRP bars were not taken into account.

The fracture energy Γ_f was first computed from Eq. (13) and then the parameter k_G was evaluated by using Eq. (14). The relevant values of Γ_f and k_G are reported in Tables 2 and 3 and appear consistent with data from the literature. Typical fracture energy values range between 0.4 N/mm and 0.8 N/mm, as confirmed, for example, by experimental tests in [31] (Γ_f = 0.77 N/mm) and in [36] (Γ_f = 0.91 N/mm). Moreover, the application of Eq. (3), (12) provides maximum shear strength values in the range between 4.0 MPa and 6.5 MPa which are in agreement with [15].

Finally, the scattering of the mode II interfacial fracture energy is not due to inaccuracy of the model which is capable to produce estimation of the bond strength and mode II interfacial fracture energy in good agreement with literature results and experimental

Table 4
Parameters of the statistical analysis of the enlarged experimental database.

Spec. type	Distribution	k_G	
		5% perc.	50% perc.
CFRP wrap	Normal	0.572	1.355
	Lognormal	0.665	1.265
CFRP strip	Normal	0.163	1.192
	Lognormal	0.481	1.058

evidences. Perhaps, it is inherent to the considered experimental set-up (shear tests) to evaluate the interface mode II fracture properties.

In Fig. 10, the experimental cumulative distribution function of k_G for FRP wraps is compared to the normal and lognormal theoretical model. Finally, in Fig. 11 the experimental cumulative distribution function of k_G for FRP strips is compared to the normal and lognormal theoretical model.

Then the experimental data are fitted under the assumption of both a normal distribution and a lognormal one. For wrap reinforcing systems, both normal and lognormal distribution models produce accurate estimation of the debonding load while for strip reinforcement systems the lognormal distribution seems more suitable. The corresponding 50% and 5% percentile values are then evaluated and reported in Table 4.

It is noticeable that, when specimens reinforced with CFRP wraps and reinforced with CFRP strips are separated, remarkably different k_G values are obtained both concerning the 50% and 5% percentile values. In general higher bond strength is expected for specimens reinforced with FRP wraps compared to FRP strips. In fact, when FRP wraps are applied, the bonding technique and the greater surface roughness of the wrap ensures an accurate application and prevents premature failures.

Experimental results and the corresponding k_G parameters are more scattered for specimens reinforced with FRP strips than for specimens with FRP wraps. Although FRP strips present a better performance in factory quality control and superior bonding skills when compared to FRP wraps, systems reinforced with FRP strips appear to be extremely sensitive to the experimental setup and parameters in bonding tests, see also [6]. Besides, the FRP strip thicknesses are almost ten times greater than the FRP wrap ones, leading to greater load misalignments possibly to premature failure, see also [7]. As a result, it may be observed that different reinforcing materials (strips or wraps) strongly influence the values of the mode II interfacial fracture energy and require different model parameters. In particular lower mode II interfacial fracture energy is required for strips reinforcements since fracture tends to be mixed mode due to the presence of out-of-plane displacements instead of single mode II.

5. Conclusions

In the present paper, experimental results on FRP reinforcements bonded to concrete were discussed in terms of fracture energy. On the basis of the concrete Mohr–Coulomb failure criterion, considerations on the specific fracture energy relationship for the maximum load transferred between FRP and concrete are presented.

The results of 30 experimental tests performed by the authors were added to experimental data selected from the literature in order to get an enlarged extensive database. A statistical analysis of the fracture energy parameter k_G was performed and the experimental data were fitted under the assumption of both normal and lognormal distribution. The statistical analyses were performed separately for strips and wraps since a different behavior of the two reinforcing systems was observed.

Experimental results and the relevant statistical analyses show that:

- In general higher bond strength was observed for specimens reinforced with FRP wraps. Pultruded strips have, in fact, a greater thickness compared to the laminated wraps. As well known, the shear and normal stresses at the FRP-concrete interface increase with the reinforcement thickness which has then a detrimental effect on the debonding performance of the FRP reinforcement.
- Experimental results clearly showed that the scatter of the strips tests is significant despite of their better factory quality control and the simplest installation compared to wraps. This is probably due to the sensitivity of this reinforcing system to the detailing of the experimental setup. In particular the debonding load for strips is sensitive to the axial alignment with the applied load. Lower mode II interfacial fracture energy is required for strips reinforcements since fracture tends to be mixed mode due to the presence of out-of-plane displacements.
- As a refinement to current bond strength and fracture energy models, statistical analyses showed that both normal and lognormal distribution models produce accurate estimation of the debonding load for wrap reinforcing systems. Lognormal distribution is more suitable for strip reinforcement systems.

The statistical analyses clearly show that wraps and strips debonding loads should be computed separately. Wraps reinforcing systems are not sensitive to the model for the allowable shear stress in the concrete substrate and to the probability distribution model. On the other hand, strips reinforcing systems should be analyzed with model I for the allowable shear stress in the concrete substrate and lognormal distribution model.

Acknowledgment

The authors acknowledge the financial support of the Italian Ministry of Civil Protection in the framework of the "Laboratories University Network of Seismic Engineering" – ReLUIS.

References

[1] Toutanji H, Ortiz G. The effect of surface preparation on the bond interface between FRP sheets and concrete members. Compos Struct 2001;53:457–62.
[2] Silva MAG, Biscaia H. Degradation of bond between FRP and RC beams. Compos Struct 2008;85(2):164–74.
[3] Karbhari VM, Zhao L. Issues related to composite plating and environmental exposure effects on composite-concrete interface in external strengthening. Compos Struct 1998;40(3):293–304.
[4] Chen JF, Teng JG. Anchorage strength models for FRP and steel plates bonded to concrete. J Struct Eng 2001;127(7):784–91.
[5] Yao J, Teng JG, Chen JF. Experimental study on FRP-to-concrete bonded joints. Composites: Part B 2005;36:99–113.
[6] Savoia M, Bilotta A, Ceroni F, Di Ludovico M, Fava G, Ferracuti B, Mazzotti C, Nigro E, Olivito R, Pecce M, Poggi C. Experimental round robin test on FRP-concrete bonding. In: Proceedings of 9th international symposium on fiber reinforced polymer reinforcement for concrete structures, Sydney, Australia; 13–15 July 2009.
[7] Bilotta A, Di Ludovico M, Nigro E. FRP-to-concrete interface debonding: Experimental calibration of a capacity model. Composites: Part B 2011;42:1539–53.
[8] Smith ST, Teng JG. Interfacial stresses in plated beams. Eng Struct 2001;23(7):857–71.
[9] Nakaba K, Kanakubo T, Furuta T, Yoshizawa H. Bond behavior between fiber-reinforced polymer laminates and concrete. ACI Struct J 2001;98(3):359–67.
[10] Wu Z, Yuan H, Niu H. Stress transfer and fracture propagation in different kinds of adhesive joints. J Eng Mech 2002;128(5):562–73.
[11] Smith ST, Teng JG. FRP-strengthened RC beams. I: review of debonding strength. Eng Struct 2002;24:385–95.
[12] Smith ST, Teng JG. FRP-strengthened RC beams. II: assessment of debonding strength models. Eng Struct 2002;24:397–417.

[13] Wu ZS, Yin J. Fracturing behaviors of FRP-strengthened concrete structures. Eng Fract Mech 2003;70(10):1339–55.
[14] Yuan H, Teng JG, Seracino R, Wu ZS, Yao J. Full-range behavior of FRP-to-concrete bonded joints. Eng Struct 2004;26:553–65.
[15] Lu XZ, Teng JG, Ye LP, Jiang JG. Bond-slip models for FRP sheets/plates bonded to concrete. Eng Struct 2005;27(4):920–37.
[16] Abdelouahed T. Improved theoretical solution for interfacial stresses in concrete beams strengthened with FRP plate. Int J Solids Struct 2006;43:4154–74.
[17] Ferracuti B, Savoia M, Mazzotti C. Interface law for FRP–concrete delamination. Compos Struct 2007;80(4):523–31.
[18] Colombi P, Fava G, Poggi C. Bond strength of CFRP–concrete elements under freeze-thaw cycles. Compos Struct 2010;92:973–83.
[19] Teng JG, Yuan H, Chen JF. FRP-to-concrete interfaces between two adjacent cracks: theoretical model for debonding failure. Int J Solids Struct 2006;43(18–19):5750–78.
[20] ASTM D3039. Standard test method for tensile properties of polymer matrix composite materials; 2008.
[21] ISO 1172. Textile-glass-reinforced plastics–prepregs, moulding compounds and laminates – determination of the textile-glass and mineral-filler content-calcination methods; 1996.
[22] SIKA Deutschland Inc., Technical datasheet; 2008.
[23] EN 3791:2008. Assessment of in situ compressive strength in structures and precast concrete components; 2008.
[24] EN 12390-4. Testing hardened concrete – compressive strength – specification for testing machines; 2002.
[25] EN 12390-6, Testing hardened concrete – tensile splitting strength of test specimens; 2002.
[26] fib Externally bonded FRP reinforcement for RC structures. fib Bulletin 14. Technical report prepared by the working party EBR of task group 9.3. International Federation for Structural Concrete; 2001.
[27] CNR (Italian National Research Council) Committee. 2006. Guide for the design and construction of externally bonded FRP systems for strengthening existing structures. CNR DT 200/2004 Technical Report [in English].
[28] Brosens K, Van Gemert D, Vandewalle L. Anchorage of externally bonded steel plates and CFRP laminates for the strengthening of concrete elements. Phd thesis, Faculteit Toegepaste Wetenschappen, Katholieke Universiteit Leuven; 2001.
[29] Blaschko M, Niedermeier R, Zilch K. Bond failure modes of flexural members strengthened with FRP. Fiber Compos. In: Saadatmanesh, Ehsani (editors), Infrastruct proc 2nd int conf on compos in infrastruct; 1996. p. 315–27.
[30] Neubauer U, Rostásy FS. Design aspects of concrete structures strengthened with externally bonded CFRP plates. In: Forde, editor. Proc 7th int conf on structural faults and repairs. Edinburgh, UK: Engineering Technics Press; 1997. p. 109–18.
[31] Chajes MJ, Finch WW, Januszka TF, Thomson TA. Bond and force transfer of composite material plates bonded to concrete. ACI Struct J 1996;93(2):295–303.
[32] Freddi F, Savoia M. Analysis of FRP–concrete debonding via boundary integral equations. Eng Fract Mech 2008;75:1666–83.
[33] Takeo K, Matsushita H, Makizumi T, Nagashima G. Bond characteristics of CFRP sheets in the CFRP bonding technique. Proc Jpn Concr Inst 1997;19(2):1599–604.
[34] Fava G, Mazzotti C, Poggi C, Savoia M. The effect of the aggressive environment on the bond strength of FRP-concrete specimens. In: Proceedings of 9th international symposium on fiber reinforced polymer reinforcement for concrete structures, Sydney, Australia; 13–15 July 2009.
[35] Ceroni F, Pecce M. Evaluation of bond strength in concrete elements externally reinforced with CFRP sheets and anchoring devices. J Compos Constr 2010;14(5):521–30.
[36] Täljsten B. Plate bonding; Strengthening of existing concrete structures with epoxy bonded plates of steel or fiber reinforced plastics. Phd thesis, Luleå University of Technology, Sweden; 1994.
[37] Mazzotti C, Savoia M, Ferracuti B. An experimental study on delamination of FRP plates bonded to concrete. Constr Build Mater 2008;22:1409–21.
[38] Bilotta A, Ceroni F, Di Ludovico M, Nigro E, Pecce M, Manfredi G. Bond efficiency of EBR and NSM FRP systems for strengthening concrete members. J Comp Constr 2011;15(5):757–72.
[39] European Commitee for Standardization. EN 1992-1-1 – Eurocode 2 – Design of concrete structures – Part 1–1: General rules and rules for buildings design of concrete structures; 2004.